KAUNAS UNIVERSITY OF TECHNOLOGY
VYTAUTAS MAGNUS UNIVERSITY

DALIA ČALNERYTĖ

# DEVELOPMENT OF MULTI-SCALE MODELS FOR DYNAMIC ANALYSIS OF UNIDIRECTIONAL COMPOSITE TEXTILES

Summary of Doctoral Dissertation
Physical Sciences, Informatics (09P)

2017, Kaunas

This doctoral dissertation was prepared at Kaunas University of Technology, Faculty of Informatics, Department of Applied Informatics during the period of 2012–2017.

**Scientific Supervisor:**
Prof. Dr. Habil. Rimantas BARAUSKAS (Kaunas University of Technology, Physical Sciences, Informatics – 09P).

**Editor:** Armandas Rumšas (Publishing Office "Technologija")

**Dissertation Defence Board of Informatics Science Field:**
Prof. Dr. Habil. Minvydas RAGULSKIS (Kaunas University of Technology, Physical Sciences, Informatics – 09P) – **chairman**;
Prof. Dr. Romas BARONAS (Vilnius University, Physical Sciences, Informatics – 09P);
Prof. Dr. Habil. Rimantas KAČIANAUSKAS (Vilnius Gediminas Technical University, Physical Sciences, Informatics – 09P);
Prof. Dr. Gintaras PALUBECKIS (Kaunas University of Technology, Physical Sciences, Informatics – 09P);
Prof. Dr. Miguel A. F. SANJUAN (Rey Juan Carlos University, Physical Sciences, Informatics – 09P).

The official defence of the dissertation will be held at 2 p.m. on 19 June, 2017 at the public meeting of Dissertation Defence Board of Informatics Science Field in the Dissertation Defence Hall at Kaunas University of Technology.

Address: K. Donelaičio St. 73-403, 44249 Kaunas, Lithuania.
Tel. no. (+370) 37 300 042; fax. (+370) 37 324 144; e-mail doktorantura@ktu.lt.

Summary of doctoral dissertation was sent on 19 May, 2017.
The doctoral dissertation is available on the internet http://ktu.edu and at the libraries of Kaunas University of Technology (K. Donelaičio St. 20, Kaunas, Lithuania) and Vytautas Magnus university (K. Donelaičio St. 52, Kaunas, Lithuania).

KAUNO TECHNOLOGIJOS UNIVERSITETAS
VYTAUTO DIDŽIOJO UNIVERSITETAS

DALIA ČALNERYTĖ

# DAUGIASKALIŲ SKAITINIŲ MODELIŲ SUKŪRIMAS LANKSČIŲ VIENKRYPČIŲ KOMPOZITŲ DINAMIKOS ANALIZEI

Daktaro disertacijos santrauka
Fiziniai mokslai, Informatika (09P)

2017, Kaunas

Disertacija rengta 2012–2017 metais Kauno technologijos universiteto Informatikos fakultete Taikomosios informatikos katedroje.

**Mokslinis vadovas:**
Prof. habil. dr. Rimantas BARAUSKAS (Kauno technologijos universitetas, fiziniai mokslai, informatika – 09P).

**Redagavo:** Rozita Znamenskaitė (leidykla „Technologija“)

**Informatikos mokslo krypties disertacijos gynimo taryba:**
Prof. habil. dr. Minvydas RAGULSKIS (Kauno technologijos universitetas, fiziniai mokslai, informatika – 09P) – **pirmininkas**;
Prof. dr. Romas BARONAS (Vilniaus universitetas, fiziniai mokslai, informatika – 09P);
Prof. habil. dr. Rimantas KAČIANAUSKAS (Vilniaus Gedimino technikos universitetas, fiziniai mokslai, informatika – 09P);
Prof. dr. Gintaras PALUBECKIS (Kauno technologijos universitetas, fiziniai mokslai, informatika – 09P)
Prof. dr. Miguel A. F. SANJUAN (Rey Juan Carlos universitetas, fiziniai mokslai, informatika – 09P).

Disertacija bus ginama viešame Informatikos mokslo krypties disertacijos gynimo tarybos posėdyje 2017 m. birželio 19 d. 14 val. Kauno technologijos universiteto disertacijų gynimo salėje.

Adresas: K. Donelaičio g. 73-403, 44249 Kaunas, Lietuva.
Tel. (370) 37 300 042; faks. (370) 37 324 144; el. paštas doktorantura@ktu.lt.

Disertacijos santrauka išsiųsta 2017 m. gegužės 19 d.
Disertaciją galima peržiūrėti internete (http://ktu.edu), Vytauto Didžiojo universiteto (K. Donelaičio g. 52, Kaunas, Lietuva) ir Kauno technologijos universiteto (K. Donelaičio g. 20, Kaunas, Lietuva) bibliotekose.

## 1. INTRODUCTION

Composite materials are materials composed of two or more materials of significantly different properties. Most of the natural materials such as wood, bones, etc. are composite materials. Artificial composites are widely used because of their ability to obtain the overall required material properties by varying the internal structure and the proportions of the constituting materials. Due to the good weight and strength ratio, composite materials are widely used in manufacturing aircraft parts, helmets, bullet-proof vests, medical equipment, etc.

Numerical simulation of the mechanical behavior of the objects and constructions made of composites by taking into account their microstructure requires unrealistically large computational resources which are not expected to be available in the near future. That is why the multi-scale approach is applied. This approach enables to define the analyzed object in different scales with the respective assumptions. In terms of the research of the problem, the top-bottom or bottom-top multi-scale method is applied [1]. In the top-bottom case, a small region is analyzed in the minute scale with the boundary conditions (e.g. displacements) transmitted from a large scale. In the bottom-top case, material properties in a large scale are obtained from the representative areas in the minute scale. The representative region is a small part of an object that can be treated as a differential element of a large scale. Usually, it is a numerical model of a micro-cube that is used to define the stress-strain relation for the average values calculated in the volume of the representative region.

The bottom-top multi-scale model of unidirectional laminated textile is analyzed in this research. The equivalent material parameters are calculated in the minute scale with respect to the representative region that takes into account the internal structure of the composite. The obtained parameters are used in the analysis of the object in the largest scale. Due to the minute internal geometry, it is assumed that the material is homogeneous in the largest scale.

In a small strain range where the stress-strain relation is linear equivalent parameters can be obtained by asymptotic homogenization [2] or by using micro-mechanical analysis of the representative region [3]. In a large strain, the range material is additionally defined by the yield stress, the tangential modulus and the strength limit. The equivalent strength limits in this research are obtained from the analysis of the representative region with the increasing strains. If contact problems are analyzed with the destruction of the object taken into account, it is important to define the proper erosion criterion for the distorted elements so that the deletion of the elements would take place neither too early nor too late. The criterion for an element to be deleted if the effective erosion (ESD) is reached is applied in numerical simulations. The algorithm enabling to define the ESD value by analyzing rectangular regions with the rotated material system is suggested in this research. This approach contains the capacity to take into account the load combinations if the object is loaded multi-axially.

## 1.1 The Object of the Research

1. Application of multi-scale models in the analysis of unidirectional composite textiles at different levels of minuteness.
2. Models of unidirectional composite structures that are used to determine the equivalent parameters of the representative internal structure defined by finite element models in the minutest scale.
3. Transverse impact on the unidirectional composite plates defined by shell elements with the material parameters obtained from the representative element in the minutest scale.

## 1.2 The Aim of the Research

The aim of the research is to create multi-scale numerical models for the dynamic analysis of unidirectional composite textiles and to determine the parameters which would describe the behavior of a composite in the macro-scale with respect to the detailed models of its internal structure.

## 1.3 The Tasks of the Research

In order to achieve the aim, the following tasks were outlined:

1. To develop multi-scale numerical models with the internal structure of the unidirectional composite described by using two-dimensional and three-dimensional finite elements in the minutest scale.
2. To define the appropriate constraints in order to identify the linear parameters, the strength and the parameters for eroding elements.
3. To verify the developed multi-scale models by analyzing the shell element model under the loads in the composite plane in the largest scale where the material parameters used for the model are the equivalent parameters obtained from the linear and non-linear analysis of the internal structure in the minutest scale.
4. To verify the developed multi-scale models by analyzing the shell element model under the transverse impact of the rigid sphere in the largest scale and comparing the obtained results with the base model. The parameters applied in the homogeneous model of the largest scale are obtained from the linear and non-linear analysis of the internal structure in the minutest scale.
5. To verify the obtained numerical results experimentally by developing a two-scale model applied to evaluate the strength of a 3D-printed item, to analyze the influence of the internal structure and to compare the numerical and experimental results of the tension and three-point bending tests.

## 1.4 The Methods of the Research

The finite element method is applied in order to obtain the linear and non-linear parameters and the criterion for eroding elements by analyzing a numerical model in the minutest scale. The static and dynamic analysis of the representative

structure is performed by employing the created programs and finite element program LS-DYNA, the results are analyzed by using MATLAB. The convergence of the models is attained by analyzing the finite element model with meshes of different minuteness. The models in the largest scale are verified by comparing them with the base models defining the same object with respect to its internal structure.

### 1.5 Scientific Novelty and Practical Relevance

The main scientific novelty of this dissertation is the extension of the methodology applied in order to obtain the equivalent parameters in the minutest scale which allows to mathematically define the element erosion criterion. In the earlier researches, multi-scale models were applied when striving to evaluate the linear parameters, the non-linear parameters and the erosion criterion which was usually chosen by empirically appealing to analogies or to scientific intuition. The practical relevance is based on the extension of the application scope of numerical models as practically acceptable results are obtained even for complex non-linear contact problems with a small number of finite elements.

### 1.6 Approbation of the Research Results

The main results of the dissertation were published in 7 scientific publications: 2 in the journals included into the list of scientific international databases (Indexed in the Web of Science with Impact Factor) and 5 publications were delivered in other international databases. The results were also presented in 6 international conferences.

### 1.7 The structure and Volume of the Dissertation

The dissertation consists of an introduction, 4 main chapters, conclusions, a list of references, a list of the author's publications and 2 appendices. The total volume of the dissertation is 92 pages, including 39 figures, 15 tables and 125 references.

## 2. REVIEW OF RESEARCH RELATED TO MULTI-SCALE MODELING OF UNIDIRECTIONAL COMPOSITE

Unidirectional composite textiles represent a group of composite materials containing long parallel fibers bonded together by a matrix material. In order to achieve a high strength-to-weight ratio, the fiber material is much stiffer than the matrix material. According to the analysis level, models of unidirectional composites are grouped into [4]:

- zero-order models – only fibers are taken into account; no matrix material is considered.
- first-order models – fiber direction and proportions of the constituting materials are considered (Figure 2.1, a).

- second-order models – the arrangement and shape (the cross-section) of fibers and proportions of the constituting materials are considered (Figure 2.1, b).
- higher-order models – the interaction between the matrix and fibers, defects and irregularities of arrangement are considered (Figure 2.1, c).

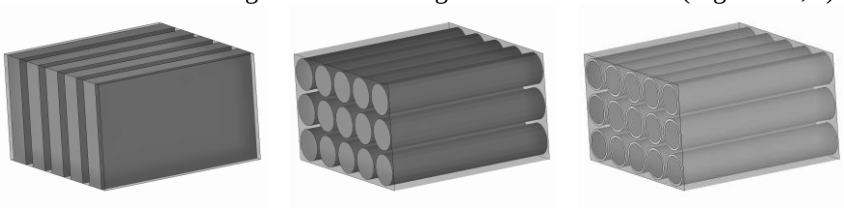

a b c

**Figure 2.1**. Models of unidirectional fiber composite: 1st order (a), 2nd order (b), higher than 2nd order (c) taking into account the interaction between the fiber and matrix materials

Due to the complex internal micro-structure, modeling unidirectional composites with respect to the internal geometry requires unreasonable computational resources. That is why multi-scale approaches are employed in order to analyze the behavior of composites. The multi-scale models are defined by the number of scales, the relations between the scales and the modeling order of the system [5].

Usually, mechanical constants of the constituting materials are known and the bottom-top approach is applied where the parameters obtained from the minutest scale model are used in the larger scale model [6]. Another multi-scale approach is to revise the solutions obtained in a large scale by analyzing the model of a particular region in a finer scale with the boundary conditions respective to a larger-scale solution [7].

In the bottom-top model, the representative volume element containing all the heterogeneities of the internal geometry is analyzed in the minutest scale [8]. Analytical formulas, micro-mechanical analysis of the finite element model and asymptotic homogenization are applied in order to evaluate the linear elastic parameters [2, 4, 9, 10]. Non-linear parameters are evaluated by using the maximum stress criterion [11] or calculated analytically with respect to the properties of the governing materials under the loading in the analyzed direction [4]. For the models where the finite element method is applied, it is necessary to define the proper boundary conditions for the representative element. Although periodic boundary conditions are recommended [3, 12, 13], the main requirement is that the analyzed region would reproduce the same behavior as a much larger structure under the same boundary conditions [13].

Another parameter applied to determine the behavior of the composite structure is the erosion strain. This proper value of the erosion strain is important

in contact problems where late deletion of the element increases the stiffness of the analyzed structure. On the other hand, if elements are deleted before their strength values are reached, this results in a weaker structure [14, 15]. Usually, elements are deleted if they cause the reduction of the time step size to the determined value or meet other criteria based on the intuition of researchers. However, no direct method is proposed when seeking to determine the criterion for the deletion of the element from the model in the analyzed scholarly literature.

A structure manufactured with a 3D printer was chosen to analyze in the experimental research due to the ability to govern the internal geometry of samples. A 3D-printed structure is a composite structure of a complex geometrical microstructure containing air gaps as well as intersections between fibers in the adjacent layers and fibers in the same layer. In case of parallel fibers, the printed structure can be regarded as a unidirectional composite material.

## 3. PRINCIPLES OF MODELING

The multiscale model bottom-top was applied in this research. The internal structure of the composite layer and the properties of its materials are known in the micro-scale and the internal structure is assumed to be ideally periodic without overlaps. Two types of internal structure models regarding the first order (Figure 3.1 (a)) and the second order (Figure 3.1 (b)) are analyzed in the micro-scale in order to determine equivalent parameters (Young's moduli, Poisson's ratios, shear moduli, strength limits and erosion strain). A behavior of a structure in the largest scale is modeled with the assumption that the material is a homogeneous orthotropic material with the parameters evaluated in the finer scale.

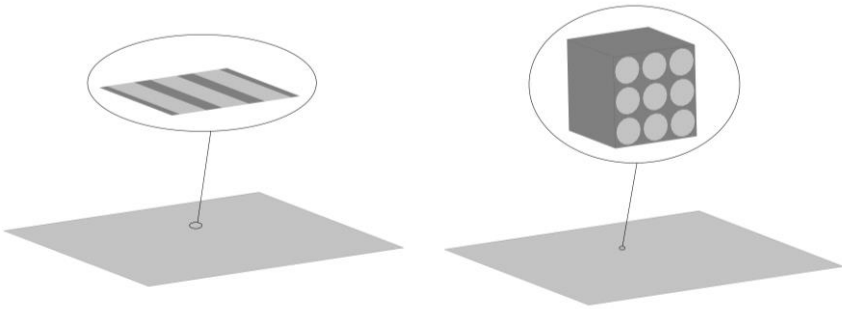

a b

**Figure 3.1**. Multi-scale models applied to modeling unidirectional fiber composites with the structure of the composite defined in the minutest scale when using the 1st order composite model (a) or the 2nd order composite model and the assumption that the material in the largest scale is a homogeneous orthotropic material

The evaluation of linear parameters is based on analyzing the representative material structure in the micro-scale. Effective stiffness tensor $D$ is valid for small

strains only and is obtained by linear relation of mean stresses over representative element σ and strains ε [9]:

$$\sigma = D\varepsilon, \tag{1}$$

where σ is a square matrix with columns representing weighted mean stresses in Voigt's notation respective to independent deformation modes, ε is a square matrix with columns representing strains of each deformation mode in Voigt's notation. Linear constants are obtained from compliance matrix $S$ which is the inverse of stiffness tensor $D$.

For the 1st order model, three pure strains are created for the representative area by prescribing boundary conditions presented in Figure 3.2 and defined by Equations (2–4). Similarly, for the 2nd order model, six pure strains are created for the representative model by prescribing boundary conditions presented in Figure 3.3 and defined by Equations (5–10). For both cases, if the strain is evaluated for the corner nodes the shear strain is pure and the obtained constants show good agreement with the values calculated by using the analytical approach or asymptotic homogenization. If straight sides are required in the deformed configuration, the calculated constants depend on the size of the analyzed region.

$$\textbf{I}: \quad u(0,y) = 0, \quad u(a,y) = \delta, \quad v(x,0) = v(x,a) = 0 \tag{2}$$

$$\textbf{II}: \quad u(0,y) = u(a,y) = 0, \quad v(x,0) = 0, \quad v(a,y) = \delta \tag{3}$$

$$\textbf{III}: \quad u(x,0) = 0, \quad u(x,a) = \delta, \quad v(0,y) = 0, \quad v(a,y) = \delta \tag{4}$$

where $\delta$ is a magnitude of displacements, and $a$ is the side length of the representative element.

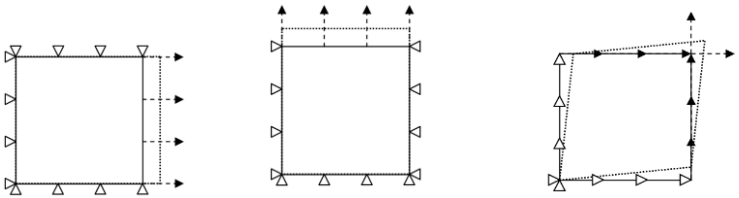

a b c

**Figure 3.2**. Load schemes for the representative element: (a) I – longitudinal tension mode, (b) II – transverse tension mode, (c) III – shear mode without the requirement that the sides of the element remain straight after deformation. The empty triangles define constraints (symbols ▷◁ mean that the node is constrained in direction X whereas symbols △▽ mean that the node is constrained in direction Y). The dotted lines represent the deformed configuration

$$\begin{aligned} &\textbf{I}: \quad u(a,y,z) = \delta, \quad u(0,y,z) = 0, \\ &\quad v(x,0,z) = v(x,a,z) = 0, \quad \omega(x,y,0) = \omega(x,y,a) = 0 \end{aligned} \tag{5}$$

$$\textbf{II}: \quad u(0,y,z) = u(a,y,z) = 0, \quad v(x,a,z) = \delta, \quad v(x,0,z) = 0, \quad \omega(x,y,0) = \omega(x,y,a) = 0 \tag{6}$$

$$\textbf{III}: \quad u(0,y,z) = u(a,y,z) = 0, \quad v(x,0,z) = v(x,a,z) = 0, \quad \omega(x,y,a) = \delta, \quad \omega(x,y,0) = 0 \tag{7}$$

$$\textbf{IV}: \quad u(x,a,z) = \delta, \quad u(x,0,z) = 0, \quad v(a,y,z) = \delta, \quad v(0,y,z) = 0, \quad \omega(x,y,0) = \omega(x,y,a) = 0 \tag{8}$$

$$\textbf{V}: \quad u(0,y,z) = u(a,y,z) = 0, \quad v(x,y,a) = \delta, \quad v(x,y,0) = 0, \quad \omega(x,a,z) = \delta, \quad \omega(x,0,z) = 0 \tag{9}$$

$$\textbf{VI}: \quad u(x,y,a) = \delta, \quad u(x,y,0) = 0, \quad v(x,0,z) = v(x,a,z) = 0, \quad \omega(a,y,z) = \delta, \quad \omega(0,y,z) = 0 \tag{10}$$

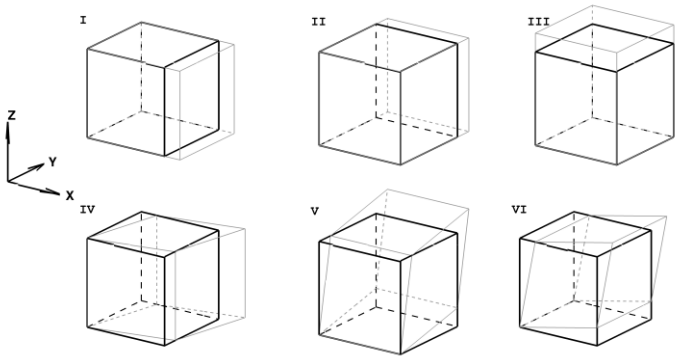


**Figure 3.3**. Schemes for creating pure strains: I – longitudinal strain mode, II, III – transverse strain mode, IV, V, VI – shear strain mode in XY, YZ, ZX planes respectively. The grey lines define the deformed object

The Hashin's failure criterion is employed in order to simulate the failure of the individual layer of the shell for the material model used in numerical experiments. This criterion determines the failure in longitudinal (fiber tension and compression) and transverse (matrix tension and compression) modes [16]:

- The fiber tension and compression modes:

$$\left(\frac{\sigma_x}{XX}\right)^2 - 1 = \begin{cases} \geq 0, failed \\ < 0, elastic \end{cases} \tag{11}$$

where $XX = \begin{cases} XT, jei\ \sigma_x \geq 0 \\ XC, jei\ \sigma_x < 0 \end{cases}$, $XT$, $XC$ are longitudinal tensile and compressive strengths.

- The matrix tension and compression modes:

$$\left(\frac{\sigma_y}{YY}\right)^2 + \left(\frac{\tau_{xy}}{SC}\right)^2 - 1 = \begin{cases} \geq 0, failed \\ < 0, elastic \end{cases} \tag{12}$$

where $YY = \begin{cases} YT, if\ \sigma_y \geq 0 \\ YC, if\ \sigma_y < 0 \end{cases}$, $YT$, $YC$ are transverse tensile and compressive strengths, and $SC$ is shear strength.

In order to apply the Hashin's failure criterion in the macro-scale, $XT$, $YT$ and $SC$ must be defined. These values are obtained by maximum stress criteria (13–15) from the analysis of the representative element by prescribing linearly increasing displacements with boundary conditions (2–4) or (5, 6, 8) respective to the order of the model. For the shear analysis, the internal structure model was surrounded with a marginal zone with the significantly higher eroding strain and width of one representative element in order to avoid the premature erosion of corner nodes which are used when calculating the strain values.

$$XT = \max_t(\sigma_x^{[t]}),\ \varepsilon_{XT} = \varepsilon_x^{[t']},\ t' : \sigma_x^{[t']} = XT \tag{13}$$

$$YT = \max_t(\sigma_y^{[t]}),\ \varepsilon_{YT} = \varepsilon_y^{[t']},\ t' : \sigma_y^{[t']} = YT \tag{14}$$

$$SC = \max_t(\tau_{xy}^{[t]}),\ \gamma_{SC} = \gamma_{xy}^{[t']},\ t' : \tau_{xy}^{[t']} = SC \tag{15}$$

The different conditions for the deletion of the shell element can significantly influence the stiffness of the structure in contact problems. The shell element is deleted if the prescribed maximum effective strain (ESD) is reached. Effective strain $ED$ combines longitudinal, transverse and shear strains in the material coordinate system [17]:

$$ED = \frac{2}{\sqrt{3}}\sqrt{3\left(\frac{\varepsilon_x+\varepsilon_y}{2}\right)^2 + \left(\frac{\varepsilon_x-\varepsilon_y}{2}\right)^2 + \gamma_{xy}^2} \tag{16}$$

The unidirectional composite is considered as *failed* if the fibers of the structure fail. This determines that the ESD values should be equal to the strain value at longitudinal strength point $\varepsilon_{XT}$ for the shell element under the longitudinal tension. However, this ESD value results in inadequately low stiffness of the structure in the model where the strains are combined. Similarly to the previous example, the fibers do not fail under the transverse tensile loading, and the ESD value for the elements under this type of loading should be equal to infinity. In case of large ESD values, the stiffness of the mezzo model is overrated, and the elements undergo unrealistically large deformations. In order to reduce the adaptation of ESD to the loading conditions, the representative element should exhibit combined strains. These conditions are created by performing explicit analysis of material samples where the material and global coordinate systems differ by various angles $\theta$ (Figure 3.4) under the loading conditions described in Figure 3.5 with increasing displacements. The sample intends to fail in the middle zone, and the failure strain of the marginal zone is significantly higher in order to avoid the material failure caused by the prescribed artificial displacements. The

samples maintain periodicity and include all the heterogeneities of the rotated micro-structure.

It is assumed that the size of the analyzed rotated element, the width of the marginal region and the mesh of the finite element model is acceptable for the evaluation of ESD values if stiffness tensor $D^{\theta}$ obtained for the model and rotated to the material coordinate system differs from stiffness tensor D calculated for the model without rotation less than the prescribed value $\epsilon$ by the means of the normed average square error:

$$R = \frac{\sqrt{\sum_{i=1}^{n}\sum_{j=1}^{n}\left(\boldsymbol{D}_{i,j}-\boldsymbol{D}_{i,j}^{\theta}\right)^{2}}}{n\cdot\max\limits_{i,j}\boldsymbol{D}_{i,j}}, \tag{17}$$

where $n$ is the number of rows (columns) in a tensor.

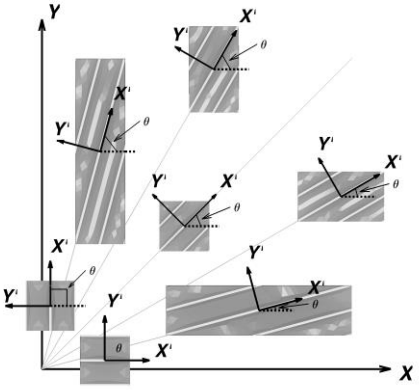


**Figure 3.4**. Analyzed models for the ESD evaluation in the coordinate system (X-Y-Z) with the material coordinate system (X'-Y'-Z). Axis Z coincides for both coordinate systems

The mean stress–strain relations are calculated for the middle zone in the global coordinate system. As the ESD is defined with respect to the direction of the fibers, the calculated stress and strain values are transferred to the material coordinate system $(X', Y', Z')$ by using the standard transformation [18]:

$$\begin{bmatrix} \sigma_{x'} & \tau_{x'y'} & \tau_{x'z'} \\ \tau_{y'x'} & \sigma_{y'} & \tau_{y'z'} \\ \tau_{z'x'} & \tau_{z'y'} & \sigma_{z'} \end{bmatrix} = \boldsymbol{\Lambda} \begin{bmatrix} \sigma_{x} & \tau_{xy} & \tau_{xz} \\ \tau_{yx} & \sigma_{y} & \tau_{yz} \\ \tau_{zx} & \tau_{zy} & \sigma_{z} \end{bmatrix} \boldsymbol{\Lambda}^{T} \tag{18}$$

where $\Lambda$ is the direction cosine matrix.

As the erosion of elements results in a steep fall of stress–strain curves, the maximum effective strain for each model is calculated at the time step before the failure of the fibers takes place. The models are classified into two groups

regarding the governing material. If the model is governed by the fibers, the stress in the fiber direction reaches the values which are close to the material strength in the fiber direction. If the model is governed by the matrix material, the stress in the transverse direction reaches the value close to the strength in the transverse direction. It is recommended to use the largest ESD value obtained for the models governed by the fibers.

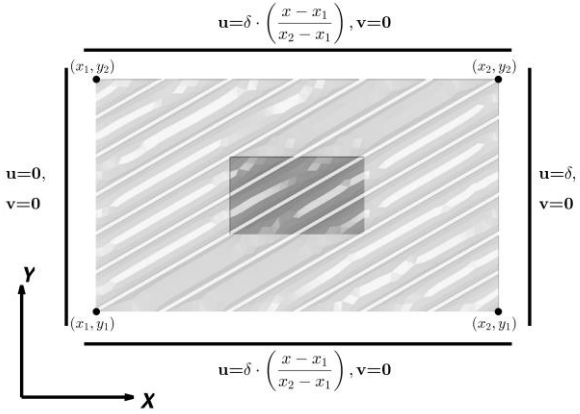


**Figure 3.5**. Boundary conditions for ESD evaluation

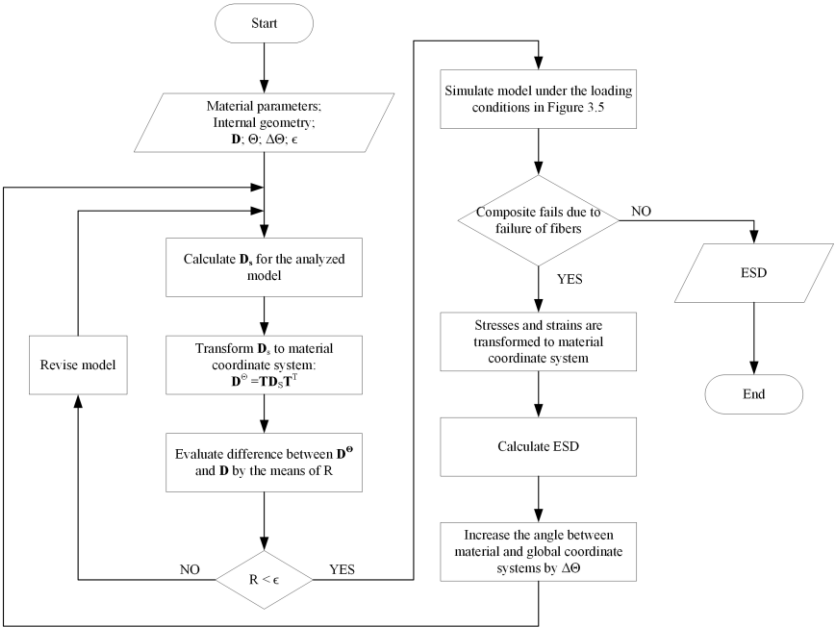


**Figure 3.6**. ESD evaluation scheme

The scheme applied in order to evaluate the ESD value is provided in Figure 3.6 and consists of two main stages defining the model creation and analysis. The input parameters are the parameters which define the behavior of the constituting materials; the internal geometry of the composite; stiffness tensor D calculated for the model without rotation; the initial rotation angle of model $\theta$ and step $\Delta\theta$; value $\epsilon$ defining the similarity of tensors D and $D^{\theta}$. It is required that the behavior of the material sample rotated by initial angle $\theta$ should be governed by the fibers.

## 4. NUMERICAL EXPERIMENTS

Low density polyethylene matrix reinforced with aramid fibers was used as a sample material combination in the micro-scale. The representative volume element analyzed in numerical experiments consists of cylindrical aramid fibers with the circular cross-section of radius $r = 4.5E-05\ m$, and the distance between the centers of adjacent fibers is $a = 1E-4\ m$. The share of fibers in the material is $\alpha_f \approx 0.6362$, the matrix share is $\alpha_m \approx 0.3638$. These share values are applied to create a representative element for the first order models.

The *MAT_PLASTIC_KINEMATIC material model (MAT_003) is employed in LS-DYNA in order to model the fiber and matrix materials with parameters in Table 4.1. The stress–strain relation of the aramid fiber is almost

linear until the failure. The matrix material, on the contrary, is elastic for small deformations only, and it undergoes large plastic deformations.

**Table 4.1**. Mechanical constants of the fiber and matrix material.

| | Fiber | Matrix |
|---|---|---|
| Young's modulus, $N/m^2$ | 9E+10 | 3E+08 |
| Poisson's ratio | 0.3 | 0.2 |
| Yield stress, $N/m^2$ | 3.5E+09 | 2E+07 |
| Density, $kg/m^3$ | 1400 | 920 |
| Failure strain | 0.001 | 0.5 |

The layer of the unidirectional fiber composite in the macro scale is simulated by using material model *MAT_LAMINATED_COMPOSITE_FABRIC (MAT_58). The linear elastic parameters, the strength points with the respective strains and the erosion strain for this material model are evaluated by using RVE in the micro-scale.

The sphere is modeled by shell elements as a rigid body. The material model *MAT_RIGID (MAT_020) is employed in order to define the sphere material with the parameters as outlined in Table 4.2. All the displacements in X and Y directions and all the rotations are constrained for the nodes of the sphere. The translational mass of the sphere is equal to the mass of the solid sphere with the mass density as indicated in Table 4.2. The CONTACT_ERODING_SURFACE_TO_SURFACE type is employed in order to define the contact interaction between the sphere and plies and between the adjacent plies.

**Table 4.2**. Mechanical constants of the rigid sphere.

| | |
|---|---|
| Young's modulus, $N/m^2$ | 1.7E+10 |
| Poisson's ratio | 0.4 |
| Density, $kg/m^3$ | 11270 |

Two types of macro-scale models are analyzed in contact with the rigid sphere and the in-plane load with the linear parameters in Table 4.3, and the strain and the strength pairs in Table 4.4. The B and C types correspond to the homogeneous orthotropic shell models with the parameters obtained while using, respectively, the 1st and 2nd order representative elements.

As the stiffness in the fiber direction is governed by fibers, the Young's moduli in the fiber direction differ by less than 5%. The stiffness in the transverse direction and the shear are governed by both constituting materials, and this results in a significant difference between the Young's moduli in the transverse direction and the shear moduli. Moreover, the parameters respective to Z direction or YZ and ZX planes are not obtained while using the first order representative model. Due to the symmetric cross-section of the fibers in YZ plane of the 2nd order model, the parameters in the transverse directions (Y and Z) are equal.

**Table 4.3**. Linear parameters used in the macro-scale model.

| | | B type | C type |
|---|---|---|---|
| Young's moduli, N/m$^2$ | $E_x$ | 5.7368e+10 | 5.5882e+10 |
| | $E_y$ | 8.5338e+08 | 1.4315e+09 |
| | $E_z$ | | 1.4315e+09 |
| Poisson's ratio | $\nu_{xy}$ | 0.2636 | 0.2729 |
| | $\nu_{yz}$ | | 0.1098 |
| | $\nu_{zx}$ | | 0.0070 |
| Shear moduli, N/m$^2$ | $G_{xy}$ | 3.6963e+08 | 5.9152e+08 |
| | $G_{yz}$ | | 3.8500e+08 |
| | $G_{zx}$ | | 5.9152e+08 |

Similarly to the linear parameters, strength $XT$ and strain $\varepsilon_{XT}$ in the fiber direction obtained for the 1st and 2nd order models differ by less than 5%, yet their values corresponding to the transverse direction and the shear differ significantly.

**Table 4.4**. Non-linear parameters used in the macro-scale model.

| | B type | C type |
|---|---|---|
| $XT$, N/m$^2$ | 2.2360e+09 | 2.2331e+09 |
| $YT$, N/m$^2$ | 3.1442e+07 | 5.5664e+07 |
| $SC$, N/m$^2$ | 1.9572e+07 | 1.3385e+07 |
| $\varepsilon_{XT}$ | 0.0392 | 0.0392 |
| $\varepsilon_{YT}$ | 0.2295 | 0.0770 |
| $\gamma_{SC}$ | 0.3213 | 0.0861 |

Figure 4.1 and Figure 4.2 show the stress–strain relations of respectively the 1st and 2nd order models of the representative regions with the material coordinate system rotated regarding the global coordinate system. The number next to the letter corresponds to the magnitude of the angle in degrees between the material and the global coordinate systems. Models B00, B15, B30, B45, B60 (Figure 4.1, a) and C00, C15, C30, C45 (Figure 4.2, a) fail due to the erosion of the fiber elements. This causes erosion in the matrix material. On the contrary, after the matrix erosion in models B75, B90, C60, C75 and C90, fibers still continue to deform. The ESD values for the models with the matrix erosion followed by the fiber erosion are significantly higher.

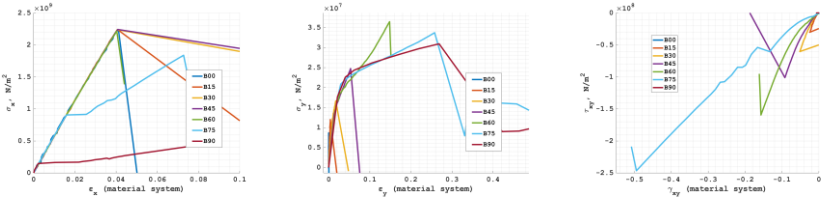


a b c

**Figure 4.1**. Longitudinal (a), transverse (b) and shear (c) stress – strain curves of the 1st order models in the material coordinate system

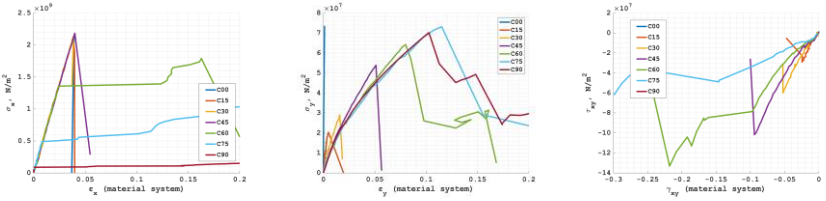


a b c

**Figure 4.2**. Longitudinal (a), transverse (b) and shear (c) stress–strain curves of the 2nd order models in the material coordinate system

ESD values calculated from the stress–strain relations in Figure 4.1 and Figure 4.2 are given in Table 4.5. For both order models, the ESD values corresponding to the same rotation angles differ by less than 10% with the notable exception of the model corresponding to 60°. Moreover, the fiber material fails earlier than the matrix material for B60 in contrast to C60 where the matrix material fails earlier. Regarding the criterion defined in Chapter 2, the ESD values corresponding to models B60 and C45 should be used in the macro scale simulations.

**Table 4.5**. ESD values.

| | 1st order models | | | | | | |
|---|---|---|---|---|---|---|---|
| | B00 | B15 | B30 | B45 | B60 | B75 | B90 |
| ESD | 0.048 | 0.057 | 0.084 | 0.142 | 0.269 | 1.275 | 3 |
| | 2nd order models | | | | | | |
| | C00 | C15 | C30 | C45 | C60 | C75 | C90 |
| ESD | 0.045 | 0.055 | 0.083 | 0.142 | 0.407 | 1.258 | 3 |

Numerical axial tension tests (Figure 4.3 – in the fiber direction, Figure 4.4 – in the transverse direction) of the homogeneous shell model with various ESD values are performed in order to verify whether the behavior of the homogeneous shell element model matches the behavior of the respective model.

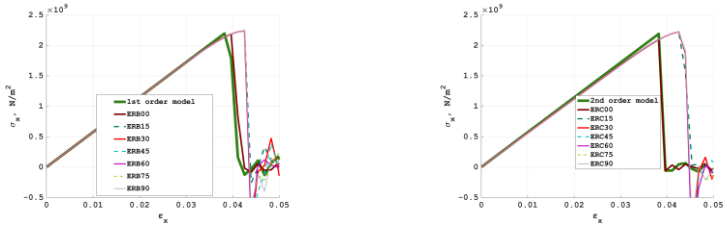


a b

**Figure 4.3**. Stress–strain curves under the tension load in the fiber direction

For both types, the homogeneous model with the ESD value corresponding to 0° rotation angle matches the base model of the respective order best of all as the boundary conditions closely match the boundary conditions which are used to calculate the ESD values.

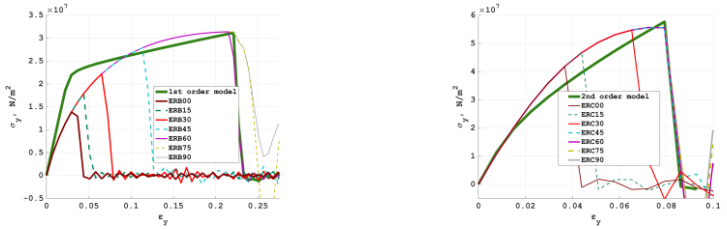


a b

**Figure 4.4**. Stress–strain curves under the tension load in the direction transverse to the fibers

As the tension in the transverse direction is governed by the matrix material, the models with the ESD values calculated for the regions governed by the matrix material fit the base model the best. Moreover, the boundary conditions used in this test are close to the boundary conditions applied when evaluating the ESD for the models with 90° rotation angles.

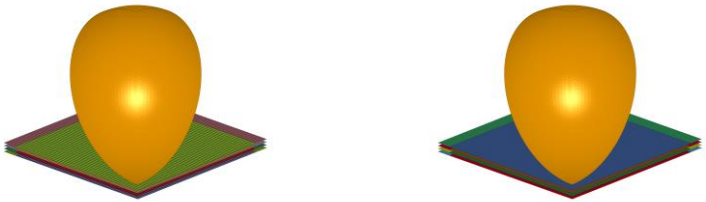

a b

**Figure 4.5**. Base model (1st order model) (a) and homogeneous shell element model (b) of 4 crossed plies in contact with a rigid sphere

The impact of the sphere at a high initial velocity (440 m/s) to the unidirectional composite is analyzed in numerical examples. Homogeneous shell models with the parameters calculated while using the 1st (B) and 2nd (C) order models are analyzed in this research. The results of a sphere perforating 1-ply or 2, 4, 8 crossed plies of homogeneous shell models are compared with the 1st order base model (Figure 4.5) by the means of the sphere velocity. The models are reduced to the quarter with the appropriate symmetry conditions. In order to avoid failure of fibers due to the boundary effects, the material in the marginal zone has significantly higher erosion values.

What regards the variation of the sphere velocity at the last analyzed time step, the models are classified in three groups. The first group corresponds to the models that are too brittle, and the variation of the sphere velocity in contact with the models is more that 10% compared with the base model. The second group refers to the models with the sphere velocity in the 10% range of the base model. Lastly, the third group corresponds to the model which is stiffer due to the late deletion of elements, and the reduction of the sphere velocity is more than 10% higher compared to the base model.

With respect to the classification described above, B type models are grouped successively: I group – ERB00, ERB15; II group – ERB30, ERB45; III group – ERB60, ERB75, ERB90. Moreover, the sphere velocity is not leveled for models ERB75 and ERB90 due to the late deletion of the elements in all the analyzed cases (Figure 4.6). Model ERB45 showed the best agreement with the base model in the transverse impact simulation of the B type models, although the suggested criterion implied that the ERB60 value would fit the base model the best.

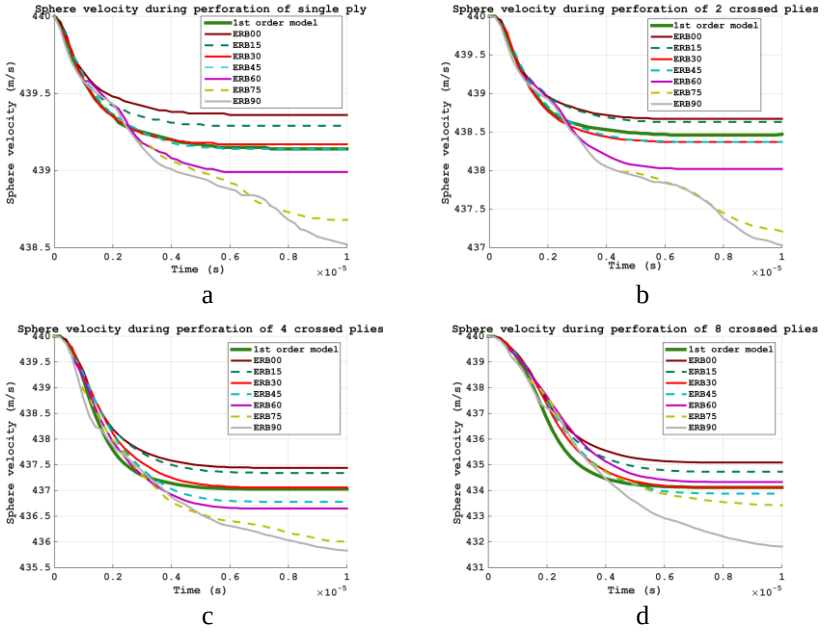


**Figure 4.6**. Comparison of the sphere velocity during the perforation of a single ply (a) and 2 (b), 4 (c), 8 (d) crossed plies while using the 1st order model and homogeneous shell models with the ESD values obtained while using the respective 1st order models for evaluation

C type models are grouped successively: I group – ERC00, ERC15; II group – ERC30, ERC45, ERC60; III group – ERC75, ERC90. Moreover, the sphere velocity is not leveled for model ERC90 due to the late deletion of elements in all the analyzed cases (Figure 4.7). For C type models, the ESD value determined by using the criteria defined above is correct as in all the analyzed cases of the transverse impact, the variation of the sphere velocity differed less than 10% from the base model.

It is important to note that in order to identify the ESD properly, the global dominant loading type should be taken into account. However, usually, it is not known in advance. That is why, the ESD value should be as universal as possible.

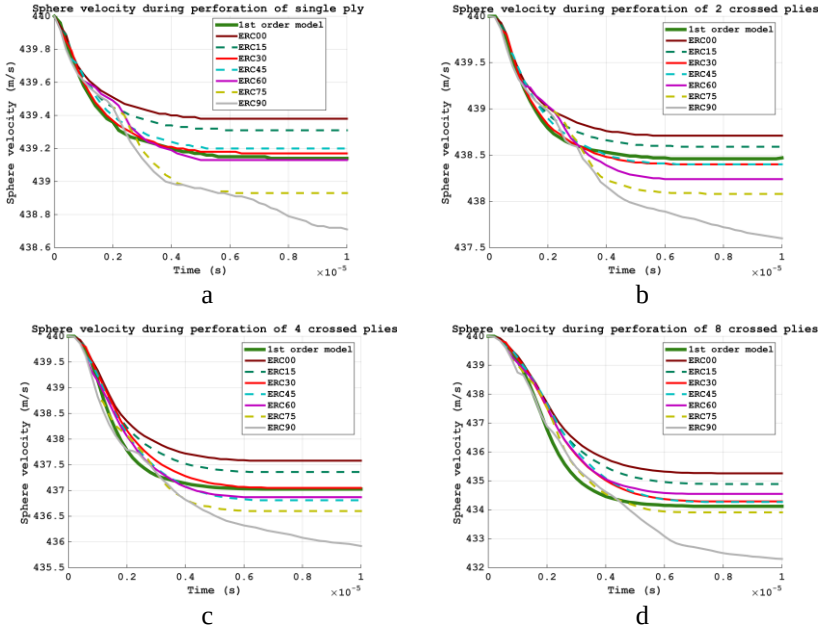


**Figure 4.7**. Comparison of the sphere velocity during the perforation of a single ply (a) and 2 (b), 4 (c), 8 (d) crossed plies when using the 1st order model and homogeneous shell models with the ESD values obtained when using the respective 2nd order models for evaluation

## 5. EXPERIMENTAL RESEARCH OF 3D-PRINTED ITEMS

The aim of this research is to investigate the influence of a geometrical microstructure on the mechanical properties of the structures manufactured by using the additive technology. A two-scale numerical model was created in order to reproduce the tension and the three-point flexure experimental results.

The idealized situation is considered in this research by assuming the representative volume element as a small periodical cell covering all the heterogeneities of the internal structure corresponding to a different layer height. The representative elements are designed after the analysis of the GCode generated by slicing software Slic3r for the 3D printed item with the layer height of 0.2 *mm*, 0.25 *mm*, 0.3 *mm*, 0.35 *mm*, 0.4 *mm*. Each micro-model consists of one full fiber surrounded by a half of the adjacent inter and intra-layer fibers. The cross-section of the fiber is approximated as a rounded rectangle (Figure 5.1).

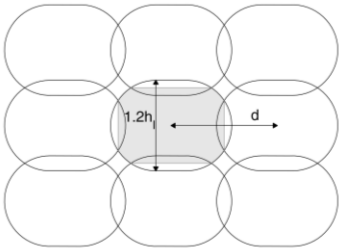


**Figure 5.1**. The geometry of the cross-section of 9 parallel fibers in the micro-scale ($h_l$– layer thickness, $d$ – distance between the centers of the adjacent fibers)

The LS-DYNA *MAT_PLASTIC_KINEMATIC material model was applied for FE models of the constant stress solid elements in the micro-scale with the parameters listed in Table 5.1.

**Table 5.1**. Material constants of the micro-scale model.

| | |
|---|---|
| Young's modulus, N/m$^2$ | 2.9E+009 |
| Poisson's ratio | 0.32 |
| Yield stress, N/m$^2$ | 3E+007 |
| Tangent modulus, N/m$^2$ | 5E+008 |
| Failure strain for eroding elements | 0.07 |

In the macro scale, the orthotropic internal micro-structure of a 3D-printed item is presented by the material model *MAT_NONLINEAR_ORTHOTROPIC applied for solid elements. The material model in the small strains range is defined by the linear stiffness tensor. At finite strains, the non-linear behavior of the material is described by nominal stress versus the strain curves in three perpendicular directions, such as the fiber direction, the transverse intra-layer direction (perpendicular to parallel fibers within a layer) and the inter-layer direction (perpendicular to the parallel adjacent layers). The shear behavior is defined by the nominal shear versus the strain curves in three orthogonal material planes.

The linear stiffness tensor was evaluated for each micro-model after prescribing small displacements regarding Equations (5–10) for the rectangular element and calculating stiffness matrix $D$ from Equation (1). The stress-strain curves were also calculated under the boundary conditions (5–10) adjusted for the rectangular element. The experimental tests were performed at a low strain rate, therefore no dynamic effects were considered. In order to avoid dynamic effects, the quasi-static implicit finite element analysis of micro-models was applied in order to determine the stress–strain relationships.

The two major groups of specimens were manufactured from PLA (polylactic acid) – one group for the tensile test (a rectangular parallelepiped of dimensions $L = 150\,mm$, $b = 10\,mm$, $h = 4\,mm$), and the other group for the

flexure test (*ISO 178*, a rectangular parallelepiped of dimensions $L = 80\ mm$, $b = 10\ mm$, $h = 4\ mm$). The flexure test sample group was divided into two subgroups in accordance with the direction of the fibers in a layer. The two types of the structure were considered where fibers filled the microstructure layer by layer in the longitudinal or transverse directions.

The numerical and experimental results were compared with respect to the value of stress $\bar{\sigma}$ in the tensile test and $\hat{\sigma}$ in the three-point bending test as:

$$\bar{\sigma} = \frac{F}{b \cdot h} \tag{7}$$

$$\hat{\sigma} = \frac{3 \cdot F \cdot Ls}{2 \cdot b \cdot h^2} \tag{8}$$

where $b$ and $h$ are the width and the height of the specimen, respectively, $Ls$ is the span length between the supporting cylinders, $F$ is the force added to deform the 3D-printed item.

In the numerical model of the tension test, the rectangular parallelepiped of dimensions $L = 80\ mm$, $b = 10\ mm$, $h = 4\ mm$ corresponding to the section between the two grips was analyzed (Figure 5.2). At a low elongation rate of 50 mm/min, no dynamic effects were taken into account. This enabled to perform quasi-static implicit analysis with the increasing load.

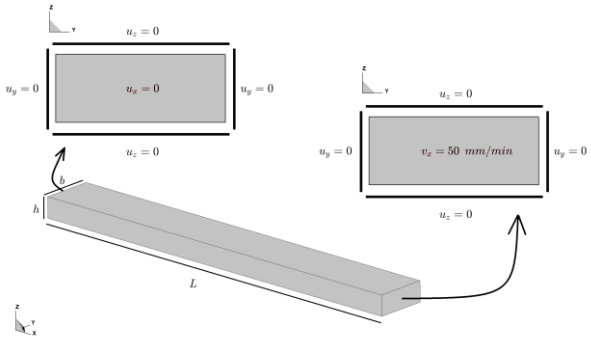


**Figure 5.2**. The finite element model for the tensile test ($u_x, u_y, u_z$ represents the displacements of the respective boundary or face; $v_x$ represents the velocity of the face)

The numerical results (Figure 5.3, b) show that the maximum $\bar{\sigma}$ ($\bar{\sigma}_{max}$) value was reached by the specimen with the parameters calculated for the micro-model with the thinnest layer and $\bar{\sigma}$ ($\bar{\sigma}_{max}$) values decrease for the models corresponding to the thicker layers. Although numerical simulations (Figure 5.3, b) imply that the structure with the thinnest layer has the highest $\bar{\sigma}_{max}$ values, the highest experimental $\bar{\sigma}_{max}$ was reached for the specimen group with 0.25 mm layer thickness (Figure 5.3, a).

The tension test is governed by the fibers and the behavior of the numerical model is similar to the input stress–strain curve obtained from the RVE in the fiber direction. As the material model used in the RVE analysis is a rough approximation of the PLA stress-strain relations, it was not possible to reproduce the behavior after the maximum point has been reached.

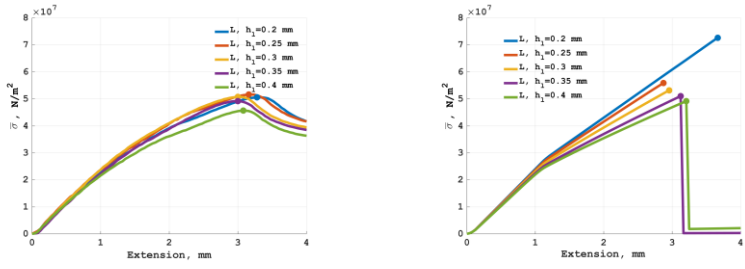


**Figure 5.3**. Typical $\bar{\sigma}$ versus the extension curves of experiments (a) and numerical simulations (b) of the tensile test with $\bar{\sigma}_{max}$ values marked for each curve

The three-point flexural test was used in order to determine the bending stiffness of the structure (Figure 5.4). The supporting and bending cylinders of the radius of 5 mm were composed of rigid shell elements (*MAT_RIGID).

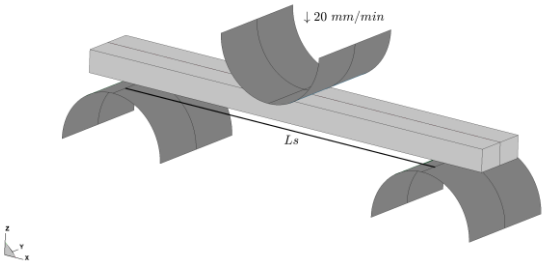


**Figure 5.4**. The finite element model for the three-point bending (flexure) test

For the specimen of the longitudinal printing direction, the highest $\hat{\sigma}_{max}$ value was simulated for the model with the thinnest layer (Figure 5.5, b). This contradicts the experimental results where the specimen with the layer height of 0.25 mm was strongest (Figure 5.5, a). The adhesion between the fibers in the same layer was poor for the samples with thin layers and did not fit the finite element model of the microstructure. However, the experimental $\hat{\sigma}$ versus the displacement curves for the other groups were arranged in the same order as the curves obtained from the numerical simulations in the analyzed range.

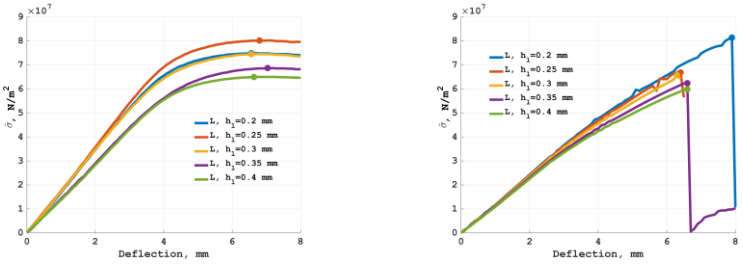


a b

**Figure 5.5**. The typical $\hat{\sigma}$ versus the deflection curves of experiments (a) and numerical simulations (b) of the flexure test for the specimen with the longitudinal printing direction with $\hat{\sigma}_{max}$ values marked for each curve

In case of a group of specimens with the transverse printing direction, the tendency that the $\hat{\sigma}_{max}$ value is higher for the specimen with the thinner layer was sustained in the numerical simulation (Figure 5.6, b). This agrees with the experimental results (Figure 5.6, a) although the experimental results for the specimen with the layers of 0.2 mm and 0.25 mm height differed insignificantly.

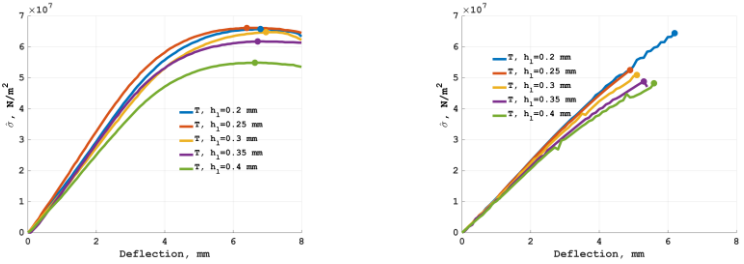


a b

**Figure 5.6**. Typical $\hat{\sigma}$ versus deflection curves of experiments (a) and numerical simulations (b) of the flexure test for a specimen with the transverse printing direction $\hat{\sigma}_{max}$ values marked for each curve

Although the simulation results showed that the $\hat{\sigma}_{max}$ value of the model increases if the structure is manufactured with a thinner layer, this contradicts the experimental results implying that the strongest structure is printed with the layer height of 0.25 mm. The limitation of the thinnest layer can be created by imprecisions of the printer and the fact that a fused material is not spread widely enough to ensure the adhesion between parallel fibers in the same layer. Moreover, the experiments demonstrated that the influence of overlaps was strongly expressed in the cases of the thinnest and the thickest layers.

## CONCLUSIONS

The multi-scale finite element model for unidirectional composite textiles was created in this research. After conducting theoretical and experimental analysis, the following conclusions were outlined:

1. Two-scale numerical models were created in order to analyze the unidirectional composite. In order to determine the parameters in the minutest scale, two models of internal composite structure respective to the first order (shell-element) model and the second order (solid-element) model were used. In the largest scale, the homogeneous shell element model is analyzed. The parameters in the fiber direction evaluated using both models differ by less than 10%, and in the transverse direction by more than 10%. That is why it is important to determine the level of minuteness in the composite analysis.
2. The boundary conditions applied in order to determine the linear parameters, the strength and the erosion strain were identified:
    2.1. Linear elastic parameters can be identified by analyzing the representative region under pure strain boundary conditions (without the straight-side restriction in the shear mode).
    2.2. Axial non-linear parameters are identified by using pure axial strain conditions with the increasing displacements. For the shear analysis, the internal structure model is surrounded with a marginal zone with significantly higher eroding strain. This modification allows to avoid the premature erosion of the corner nodes which are used to calculate the strain values.
    2.3. In order to evaluate erosion strains, models respective to the rotated material samples are analyzed. The models are surrounded with a marginal zone with significantly higher eroding strains. The axial loading test is performed for the whole structure by prescribing displacements for the wall in the loading direction and sides.
3. Axial in-plane numerical experiments in the largest scale show that the linear parameters, the strength and the effective strain value used in the element erosion criterion (calculated from the model rotated by 45° for the first order models and 60° for the second order models) were chosen properly as those models correspond to the behavior of the base model.
4. The homogeneous shell model with the eroding strain obtained when using a 45° rotated representative model showed the best agreement with the base model in the numerical analysis of transverse impact under the contact with the rigid sphere.
5. The behavior of a numerical 3D-printed item model agrees with the experimental results until the maximum stress values have been reached for the items with the mean layer heights where the appropriate adhesion between parallel printing lines is guaranteed.

## REFERENCES


1. GEISER, J. Multicomponent and Multiscale Systems. Springer International Publishing, 2016. ISBN 9783319151168.
2. PINHO-DA-CRUZ, J., OLIVEIRA, J. A. and TEIXEIRA-DIAS, F. Asymptotic homogenisation in linear elasticity. Part I: Mathematical formulation and finite element modelling. Computational Materials Science. 2009. Vol. 45, no. 4, p. 1073–1080. DOI 10.1016/j.commatsci.2009.02.025.
3. XIA, Zihui, ZHANG, Yunfa and ELLYIN, Fernand. A unified periodical boundary conditions for representative volume elements of composites and applications. International Journal of Solids and Structures. 2003. Vol. 40, no. 8, p. 1907–1921. DOI 10.1016/S0020-7683(03)00024-6.
4. VASILIEV, V.V. and MOROZOV, E.V. Advanced mechanics of composite materials. Elsevier Science, 2007. ISBN 0080453724.
5. INGRAM, G. D., CAMERON, I. T. and HANGOS, K. M. Classification and analysis of integrating frameworks in multiscale modelling. Chemical Engineering Science. 2004. Vol. 59, no. 11, p. 2171–2187. DOI 10.1016/j.ces.2004.02.010.
6. CALNERYTE, D. and BARAUSKAS, R. Multi-scale evaluation of the linear elastic and failure parameters of the unidirectional laminated textiles with application to transverse impact simulation. Composite Structures. 2016. Vol. 142, p. 325–334. DOI 10.1016/j.compstruct.2016.01.104.
7. OTERO, F., MARTINEZ, X., OLLER, S. and SALOMÓN, O. An efficient multi-scale method for non-linear analysis of composite structures. Composite Structures. 2015. Vol. 131, p. 707–719. DOI 10.1016/j.compstruct.2015.06.006.
8. PELISSOU, C., BACCOU, J., MONERIE, Y. and PERALES, F. Determination of the size of the representative volume element for random quasi-brittle composites. International Journal of Solids and Structures. 2009. Vol. 46, no. 14-15, p. 2842–2855. DOI 10.1016/j.ijsolstr.2009.03.015.
9. BARBERO, E. Finite element analysis of composite materials. Boca Raton, FL : CRC Press, 2008. ISBN 9781420054330.
10. HASSAN, E. M., GEORGIADES, A. V., SAVI, M. A. and KALAMKAROV, A. L. Analytical and numerical analysis of 3D grid-reinforced orthotropic composite structures. International Journal of Engineering Science. 2011. Vol. 49, no. 7, p. 589–605. DOI 10.1016/j.ijengsci.2011.02.004.
11. RIBEIRO, M. L., TITA, V. and VANDEPITTE, D. A new damage model for composite laminates. Composite Structures. 2012. Vol. 94, no. 2, p. 635–642. DOI 10.1016/j.compstruct.2011.08.031.

12. SEARLES, K., ODEGARD, G. and KUMOSA, M. Micro- and mesomechanics of 8-harness satin woven fabric composites: I - Evaluation of elastic behavior. Composites - Part A: Applied Science and Manufacturing. 2001. Vol. 32, no. 11, p. 1627–1655. DOI 10.1016/S1359-835X(00)00181-0.
13. JIN, K.-K., YUANCHEN, Huang, LEE, Y.-H. and SUNG, Kyu Ha. Distribution of Micro Stresses and Interfacial Tractions in Unidirectional Composites. Journal of Composite Materials. 2008. Vol. 42, no. 18, p. 1825–1849. DOI 10.1177/0021998308093909.
14. SUDHIR SASTRY, Y. B., BUDARAPU, P. R., KRISHNA, Y. and DEVARAJ, S. Studies on ballistic impact of the composite panels. Theoretical and Applied Fracture Mechanics. 2014. Vol. 72, no. 1, p. 2–12. DOI 10.1016/j.tafmec.2014.07.010.
15. BARAUSKAS, R. and ABRAITIENE, A. Multi-resolution finite element models for simulation of the ballistic impact on non-crimped composite fabric packages. Composite Structures. 2013. Vol. 104, p. 215–229. DOI 10.1016/j.compstruct.2013.04.014.
16. SCHWEIZERHOF, K, WEIMAR, K, MUNZ, Th and ROTTNER, Th. Crashworthiness Analysis with Enhanced Composite Material Models in LS-DYNA – Merits and Limits. 5th International LS-DYNA users conference. 1998.
17. TOMLIN, O. and REYNOLDS, N. Validation of a Thermoplastic Composite Material Model for Low Carbon Vehicle Applications. In : 9th European LS DYNA Conference. 2013.
18. ZIENKIEWICZ, O. C. and TAYLOR, R. L. The Finite Element Method. 2005. ISBN 9780750663212.

## LIST OF PUBLICATIONS ON THE SUBJECT OF DISSERTATION

**Articles Published in Journals Belonging to Scientific International Databases (Indexed in the Web of Science with Impact Factor):**

1. Rimavicius, V., Calneryte, D., & Barauskas, R. (2013). Coupling of zones with different resolution capabilities in dynamic finite element models of woven composites. *Mechanics*, *19*(3), 288–295.
2. Calneryte, D., & Barauskas, R. (2016). Multi-scale evaluation of the linear elastic and failure parameters of the unidirectional laminated textiles with application to transverse impact simulation. *Composite Structures*, *142*, 325–334.

**Publications in Other International Databases:**

3. Calneryte, D., & Barauskas, R. (2015). Dynamic Analysis of 4-Node Degenerated Shell Element with Updated Thickness. In *Information and Software Technologies* (pp. 592–603). Springer International Publishing.

4. Calneryte, D., & Barauskas, R. (2015). Modelling Physical Behaviour of the Unidirectional Composite Materials with FEM Using Reduced Data. *Baltic Journal of Modern Computing*, *3*(1), 16.
5. Čalnerytė, D., & Barauskas, R. (2014). Shell Failure Simulation Using Master-Slave and Penalty Methods. In *Information and Software Technologies* (pp. 408–418). Springer International Publishing.
6. Čalnerytė, D., & Barauskas, R. (2013). Two Scale Modeling of Heterogeneous Solid Body by Use of Thick Shell Finite Elements. In *Information and Software Technologies* (pp. 322–333). Springer Berlin Heidelberg.
7. Calneryte, D. (2012). Evaluation of Elasticity Parameters for Heterogeneous Material with Periodic Microstructure. In *Information and Software Technologies*(pp. 101–107). Springer Berlin Heidelberg.

## INFORMATION ABOUT THE AUTHOR OF THE DISSERTATION

**Education:**

2006–2010: Bachelor's degree in mathematics at Kaunas University of Technology, Faculty of Fundamental Sciences.

2010–2012: Master's degree (*cum laude*) in mathematics at Kaunas University of Technology, Faculty of Fundamental Sciences.

2012–2016: doctoral studies in informatics at Kaunas University of Technology, Faculty of Informatics.

**Work experience:**

Since 2015: Lecturer at Kaunas University of Technology, Faculty of Informatics.

**E-mail:**

dalia.calneryte@ktu.lt

## REZIUMĖ

Kompozicinėmis vadinamos medžiagos, sudarytos iš kelių medžiagų, kurių savybės reikšmingai skiriasi tarpusavyje. Natūralioje aplinkoje (gamtoje) daugelis medžiagų yra kompozicinės – medis, kaulai ir pan. Dirbtinės kompozicinės medžiagos plačiai naudojamos dėl galimybės kombinuojant keletą medžiagų ir parenkant tinkamą vidinę struktūrą gauti pageidaujamas visumines medžiagos savybes. Dėl parinkto gero masės ir stiprumo santykio kompozicinės medžiagos taikomos daugelyje sričių – lėktuvų, šalmų, neperšaunamų drabužių, sporto ir medicininių įrenginių gamyboje.

Skaitinių modelių, kuriais išsamiai aprašoma kompozicinių kūnų bei konstrukcijų fizikinė elgsena, mikrolygmenyje (t. y. modelyje smulkiai pavaizduojant jų mikrostruktūrą) panaudoti praktiškai neįmanoma dėl ribotų kompiuterinių išteklių. Kompiuterio ištekliai, reikalingi realių sistemų modeliavimui mikrolygmenyje, yra tiek dideli, kad netgi aprėpiamoje ateityje tokių uždavinių išspręsti greičiausiai nepavyks. Todėl praktiškai taikomi daugiaskaliai modeliai. Juose tiriami objektai pavaizduojami skirtingose skalėse, kiekvienoje jų taikant skalės skiriamąją gebą atitinkančias prielaidas. Gali būti modeliuojama nuo smulkiausios skalės iki stambiausios, arba atvirkščiai [1]. Modeliuojant nuo stambiausios skalės smulkiausios link, smulkesnėje skalėje nagrinėjamas nedidelis posritis. Jam taikomos kraštinės sąlygos pagal stambioje skalėje gaunamus sprendinius. Pavyzdžiui, smulkioje skalėje tiriamų posričio kraštinių poslinkiai gali būti priimami pagal stambioje skalėje gautus atitinkamų taškų poslinkius. Modeliuojant nuo smulkiausios skalės stambiausios link, medžiagos savybės stambioje skalėje nustatomos pagal smulkesnėje skalėje gautų tos medžiagos reprezentatyviųjų posričių (RP) sprendinius. Kūno reprezentatyviuoju posričiu (RP) vadinama mikroskalėje pavaizduota kūno dalis, kurią apytiksliai galime traktuoti kaip jo diferencialinį elementą stambioje skalėje. Dažniausiai tai būna mikrokubo geometrinės formos skaitinis modelis, pagal kurį nustatomas įtempių ir deformacijų vidutinių reikšmių ryšys, kai vidurkiai apskaičiuojami RP tūrio ribose.

Šiame darbe tiriamas daugiaskalis vienkrypčio lankstaus kompozito modelis, kai iš medžiagos struktūrą smulkioje skalėje įvertinančio RP modelio apskaičiuojami medžiagos savybes apibūdinantys parametrai, kurie vėliau taikomi modeliui stambioje skalėje nagrinėti. Tariama, jog medžiagos vidinės sandaros mikrogeometrija tiek smulki, kad stambioje skalėje medžiagą galima apytiksliai nagrinėti kaip homogeninę.

Tiesinio tamprumo ribose, kai struktūra patiria mažas deformacijas, o įtempius ir deformacijas tiesiškai sieja apibendrintasis Huko dėsnis, medžiagos parametrus galima nustatyti taikant asimptotinį homogenizavimą pagal baigtinių elementų (BE) metodu gautus sprendinius [2] arba taikant mikromechaninę modelio analizę [3]. Esant didelėms deformacijoms bei netiesinėms kompozitą sudarančių medžiagų savybėms, medžiagos elgsena stambioje skalėje gali būti

papildomai apibūdinama takumo riba, stiprėjimo moduliu bei stiprumo riba. Šiame darbe siūloma ekvivalentų medžiagos stiprumą nustatyti pagal RP tyrimo rezultatus, laipsniškai sukeliant didesnes RP deformacijas. Sprendžiant medžiagos suirimo uždavinius svarbu parinkti tinkamą algoritmą pernelyg deformuotiems baigtiniams elementams panaikinti. Kriterijus parenkamas taip, kad elementas nebūtų panaikinamas per anksti. Šiame darbe elementų panaikinimui įvedamas kriterijus, kai efektyvioji deformacija pasiekia nustatytą ribą – efektyviąją suirimo deformaciją (ESD). Šį parametrą siūloma įvertinti iš įvairiais kampais globaliojoje koordinačių sistemoje pasukto tempiamo medžiagos fragmento modelio. Taip gaunamos galimos deformacijų kombinacijos, kai struktūra veikiama nepagrindinėmis medžiagos koordinačių ašių kryptimis.

**Uždavinio formulavimas (tyrimo objektas)**

1. Daugiaskaliai modeliai, skirti nagrinėti lankstų vienkryptį kompozitą skirtingos skiriamosios gebos skalėse.
2. Vienkrypčių kompozitų struktūros modeliai, skirti stambioje skalėje taikomų ekvivalenčiųjų medžiagos parametrų nustatymui pagal reprezentatyvųjį posritį smulkioje skalėje vaizduojančius baigtinių elementų modelius.
3. Smūginio poveikio vienkrypčio kompozito plokštelėms, aprašomoms kevalo elementais, tyrimas taikant sukurtus daugiaskalius modelius.

**Tyrimo tikslas**

Sukurti lanksčių vienkrypčių kompozitų dinamikos analizei skirtus daugiaskalius modelius, kurie leistų nustatyti parametrus, apibūdinančius kompozito elgseną stambioje skalėje pagal kompozito struktūros modelius smulkiausioje skalėje.

**Tyrimo uždaviniai**

Darbo tikslui pasiekti iškelti tokie uždaviniai.

1. Sudaryti daugiaskalius skaitinius modelius, kai smulkiausioje skalėje nagrinėjama vienkrypčio kompozito struktūra aprašoma dvimačiais ir trimačiais baigtiniais elementais.
2. Apibrėžti tinkamas kraštines sąlygas tiesinių tamprumo, stiprumo ir suirimo parametrų nustatymui.
3. Verifikuoti sukurtus daugiaskalius modelius, plokštumoje tiriant stambioje skalėje kevaliniais baigtiniais elementais aprašytą modelį, kuriame panaudoti pagal smulkiausios skalės modelio tiesinės ir netiesinės analizės rezultatus gauti ekvivalenčiosios medžiagos parametrai.
4. Verifikuoti sukurtus daugiaskalius modelius, sprendžiant absoliučiai kietos sferos ir stambioje skalėje pavaizduoto kompozito smūgio sąveiką

bei sulyginant rezultatus su rezultatais, gautais naudojant smulkioje skalėje pateiktą atskaitos modelį.

5. Eksperimentiškai patikrinti, kaip skaičiavimai atitinka tikrovę, sudarant dviejų skalių modelį trimačiu (3D) spausdintuvu pagaminto objekto stiprumo tyrimui, ištirti mikrostruktūros įtaką bei sulyginti gautus rezultatus su fizikinių eksperimentų rezultatais.

**Tyrimų metodika**

Baigtinių elementų metodu iš smulkiausios skalės modelio apskaičiuojami tiesiniai ir netiesiniai tamprumo parametrai, parenkamas baigtinių elementų panaikinimo kriterijus. Statinė ir dinaminė reprezentatyvaus elemento analizė atliekama taikant sukurtas programas bei baigtinių elementų programą LS-DYNA, rezultatai apdorojami MATLAB programa. Modelių konvergavimas tiriamas keičiant baigtinių elementų skaidymo smulkumą. Modeliai verifikuojami lyginant modelius, kai ta pati konstrukcija pateikiama skirtingos skiriamosios gebos skalėse.

**Darbo mokslinis naujumas ir praktinė reikšmė**

Svarbiausias darbo mokslinio naujumo elementas yra ekvivalenčiųjų kompozicinės medžiagos parametrų nustatymo metodo išplėtimas, leidžiantis matematiškai nustatyti jos suirimo kriterijus. Iki šiol žinomuose darbuose daugiaskalės analizės būdu būdavo apskaičiuojami tiesiniai tamprumo parametrai, o netiesiniai – dažniausiai parenkami empiriškai, remiantis analogijomis bei moksline intuicija. Praktinę reikšmę sąlygoja kompozitų skaitinių modelių galimybių išplėtimas. Net ir sudėtingų netiesinės sąveikos uždavinių atveju sutaupomi skaičiavimo ištekliai, kadangi praktiškai priimtino tikslumo rezultatai gaunami esant palyginti nedideliam baigtinių elementų skaičiui.

**IŠVADOS**

Sukurtas daugiaskalis skaitinis modelis lanksčių vienkrypčių kompozitų analizei. Atlikus teorinius tyrimus ir skaitinius eksperimentus suformuluotos išvados.

1. Darbe sudaryti dviejų skalių skaitiniai modeliai vienkrypčio kompozito tyrimui. Smulkioje skalėje vienkrypčio kompozito parametrų nustatymui iš reprezentatyviojo elemento taikomi du išsamumo lygiai – sudaromi pirmos (dvimačių elementų) ir antros eilės (tūrinių elementų) kompozito modeliai. Stambioje skalėje homogeninės medžiagos modelis sudaromas iš kevalo elementų. Pagal skirtingų eilių modelius nustatyti parametrai gijų kryptimi skiriasi mažiau nei 10 %, statmenomis kryptimis – daugiau nei 10 %. Todėl kompozito struktūros analizėje svarbu tinkamai parinkti smulkiausios skalės išsamumo lygį.

2. Apibrėžtos reprezentatyvios srities modelio kraštinės sąlygos tiesinių, stiprumo ir suirimo parametrų nustatymui smulkioje skalėje.

   2.1. Tiesiniai tamprumo parametrai gali būti vertinami iš reprezentatyviojo modelio, kuriam sukurtos grynosios deformacijos (šlyties deformacijos atveju nereikalaujant, kad kraštinės po deformacijos išliktų tiesios), analizės.

   2.2. Ašiniai netiesiniai parametrai įvertinami sukuriant grynąsias ašines deformacijas su didėjančiais poslinkiais. Šlyties stiprumui nustatyti modelis turi būti papildytas aplinkinės srities elementais su kur kas didesnėmis ištrynimo deformacijomis išvengiant ankstyvo kampinių mazgų ištrynimo.

   2.3. Suirimo parametrų nustatymui taikomi pasuktų medžiagos fragmentų modeliai, patalpinti į aplinkinę sritį su kur kas didesnėmis deformacijomis. Šiems modeliams sukuriamos grynosios deformacijos, kai poslinkiai nurodomi tempiamai ir šoninėms sienoms, taip išvengiant įtempių koncentracijos reprezentatyvios srities viduje.
3. Iš kompozito plokštelių ašinių tempimo eksperimentų stambioje skalėje nustatyta, kad šiems testams tiesiniai tamprumo, stiprumo parametrai ir suirimo kriterijui taikoma deformacijos vertė parinkta tinkamai (pirmos eilės modeliams – iš modelių, pasuktų 60°, antros eilės – iš modelių, pasuktų 45° kampu), nes modeliai atitinka atskaitos modelio elgseną.
4. Iš absoliučiai kietos sferos kontakto su kompozito plokštelėmis skaitinių eksperimentų nustatyta, kad geriausiai sferos greičio kitimą dėl kontakto su atskaitos modeliu atitinka modeliai, kurių ištrynimo deformacija apskaičiuojama 45° kampu pasuktam medžiagos fragmentui.
5. Eksperimentiškai nustatyta, kad skaitinis trimačiu (3D) spausdintuvu pagaminto objekto modeliavimas atitinka eksperimentinius rezultatus iki maksimalios įtempių ribos vidutinio sluoksnio storio objektams, kurių atveju užtikrinamas tinkamas gretimų gijų susiliejimas eksperimentiniuose gaminiuose.

UDK 519.6+677-486.2](043.3)

SL344. 2017-05-08, 2,25 leidyb. apsk. l. Tiražas 50 egz.
Išleido Kauno technologijos universitetas, K. Donelaičio g. 73, 44249 Kaunas
Spausdino leidyklos „Technologija“ spaustuvė, Studentų g. 54, 51424 Kaunas